Heliyon

ELSEVIER

Received:
18 November 2018
Revised:
2 January 2019
Accepted:
11 March 2019

Cite as: Mohanraj Murugesan, Dong Won Jung. Two flow stress models for describing hot deformation behavior of AISI-1045 medium carbon steel at elevated temperatures. Heliyon 5 (2019) e01347. doi: 10.1016/j.heliyon.2019.e01347

Two flow stress models for describing hot deformation behavior of AISI-1045 medium carbon steel at elevated temperatures

Mohanraj Murugesan, Dong Won Jung *

Department of Mechanical Engineering, Jeju National University, 1, Ara 1(il)-dong, Jeju-si, Jeju-do 63243, South Korea

* Corresponding author.
E-mail address: jdwcheju@jejunu.ac.kr (D.W. Jung).

Abstract

In materials processing, practical understanding of materials behavior at elevated temperatures and high strain rates is necessary for modeling the real system behavior. The tensile deformation behavior of AISI-1045 steel material is investigated at deformation temperatures (923−1223 K) and strain rates (0.05−1.0 s^{-1}). This paper proposes a detailed research to characterize the material flow behavior based on modified Johnson-Cook (JC) and Zerilli-Armstrong (ZA) models, respectively, as well as the predictability of these two models are discussed. The experimental flow stress-strain data are employed to fit the constitutive equations to estimate the elected model material parameters. To demonstrate the validity and the accuracy of the proposed models, the model adequacies such as coefficient of determination and average absolute relative error are discussed. From the observation made, the authors found that the modified ZA model is more appropriate for predicting the material behavior as the predicted flow stress data and the experimental data displayed better correlation among them. To make this point more concrete, random experiments are conducted to validate the proposed constitutive models and the obtained results also show that the developed modified ZA model exhibits a better relationship with the experimental data. Overall, the proposed research work can be used as an efficient

https://doi.org/10.1016/j.heliyon.2019.e01347

tool in the initial design of numerical model to accurately replicate the experiment in order to save time and cost.

Keywords: Mechanical engineering, Materials science

1. Introduction

Usage of AISI-1045 medium carbon steel has continued to increase due to their excellent properties of good weldability, superior machinability and wear resistance. In addition, it can be hardened (heat to 1093−1123 K) through the heat treatment processes and also has a better forgeability (heat to 1123−1523 K) which are important features that can be used for manufacturing large section structures. The products with certain shapes, size and strength are usually achieved from the metal forming process such as rolling, extrusion, tool cutting, spinning, incremental sheet forming, etc. under hot working conditions [1,2,3]. Generally, the material behavior under hot deformation conditions are explained using the flow stress models in which the deformations conditions to alter the micro-structural evolution during the forming process are primarily explained considering strain, strain rate and temperature parameters. Even though, the flow stress models are break down into different categories such as physically-based, empirical and semi-empirical, the aim of these models to achieve the accurate prediction of the material behavior for a specific material remains same [4]. The flow stress models such as physically-based and empirical models can provide more accurate representation of the material deformation behavior over a wide range of temperatures and strain rates [5,6,7,8,9]. However, each model has its own disadvantages, for example, physically-based models often require more experimental data and high computational time for the material constants estimation. But, the empirical model, JC, can be modified to increase the predictability of the proposed model as well as the model can be incorporated into readily available commercial finite element software, where ZA model has a ability to consider the coupled effect of strain rate and temperature to predict the deformation behavior. Recently, it is proved that the artificial neural network model is capable of solving highly non-linear problems and also the model has an ability to understand the complex and non-linear relationships of stress, strain, strain rate and deformation temperature [10]. So, developing a proper flow stress model for the design process is essential to predict the materials deformation behavior at high strain rates and deformation temperatures and as a result, reasonable research has been performed considering various materials [11,12,13,14,15,16,17,18].

In the material processing, theoretical constitutive models are generally used to describe the material behavior considering the combined effects of strain hardening, strain rate hardening and thermal softening at different strain rates and deformation

 https://doi.org/10.1016/j.heliyon.2019.e01347

temperatures [19,20,21,22]. Understanding the behavior of ductile materials is essential for modeling the actual structural behavior in terms of numerical model using finite element(FE) tools. In an alternative way, it is recognized that this is the foundation of numerical modeling in FE tools to solve the actual thermal-mechanical behavior of the materials accurately. Because an appropriate flow stress model has the capability to mathematically characterize the mechanical properties and their responses for wide range of loading conditions. The reason for employing the constitutive models is that most of the model parameters are determined systematically by fitting the measured flow stress values. Therefore, the developed constitutive models can have the capability to accurately characterize the material flow behavior. Johnson and Cook proposed the JC flow stress model for metals to characterize the ductile material behavior under large deformation conditions [23]. However, it is important to note down that the combined effects of strain and strain rate hardening and thermal softening are independent of each other, which means the coupled effects are not accounted, in the original JC model. Due to the aforementioned issue, there was a possibility of losing the prediction accuracy of material flow stress values, which acquired from the original JC model [24].

Several flow stress models have been proposed to explain the material deformation behavior at different loading conditions. Guang et al. [25] utilized the modified JC model for predicting the flow behavior of 7050-T7451 aluminium alloy material for the aerospace and the automotive applications. From the comparison of the estimated and actual flow stress data, they concluded that the work hardening and thermal softening behaviors of 7050 alloy material were well explained using the modified JC model. Hongyi et al. [26] modeled the flow behavior of a β titanium alloy using the modified ZA and original JC models for the aerospace applications. From overall results, the modified ZA model was found to be more appropriate for describing the material flow behavior compared with the experimental observations. Uma et al. [27] developed a constitutive formulation of AA7075-T6 material using modified JC and modified ZA flow stress models for machining process. They made a conclusion that the prediction of flow stress from both models were quite satisfactory. But from the machining process validation using JC material constitutive model, they stated that the numerical results were not well compared with the experimental data. Dipti et al. [28] employed Arrhenius-type constitutive, modified ZA and JC models to develop the flow stress model of modified 9Cr-1Mo steel for next generation nuclear reactor applications. They reported that the modified ZA and Arrhenius-type constitutive models were in good agreement with the measured data. However, the Arrhenius-type constitutive model found to trace the deformation behavior more preciously than other models. From literature survey, it is identified that there are only few published information on the constitutive modeling of AISI-1045 steel material at high strain rates and elevated temperatures is available. Therefore, the investigation of AISI-1045 steel material at high strain rates and elevated temperatures is presented

Table 1. Chemical Composition of AISI-1045 medium carbon steel (in wt.%).

C	Fe	Mn	P	S
0.42-0.50	98.51-98.98	0.60-0.90	≤ 0.04	≤ 0.05

in this research to predict the material deformation behavior for the metal forming applications.

This present work aims to evaluate and formulate the flow behavior of AISI-1045 steel at elevated temperatures by conducting isothermal uniaxial tensile experiments over a practical range of deformation temperatures (923−1223 K) and strain rates ($0.05-1.0\,s^{-1}$). For this purpose, based on the literature survey, the two flow stress models such as the modified JC and the modified ZA models are chosen. As well as the comparative study on the selected models are conducted in order to discuss their capability to predict the material flow behavior accurately. The advantage of the proposed modified JC and the modified ZA models is that it can be successfully incorporated into several FE tools to characterize the material deformation behavior. Finally, the proposed model adequacies are evaluated statistically by comparing the values of coefficient of determination (R^2), the average absolute relative error (AARE) that determined from the measured and the estimated observations.

2. Experimental

The AISI-1045 medium carbon steel material is investigated in the present research work and the chemical composition (in wt.%) of the material is outlined in Table 1. The specimens are prepared by the water jet cutting process from the AISI-1045 steel plates and further utilized in the uniaxial tensile tests to obtain the flow stress-strain data for characterizing the hot deformation flow behavior. In detail, the tensile test specimens are prepared with the gauge-length of 25 mm with the thickness of 3 mm according to the ASTM-E8M-subsize standard. The tensile tests are performed at the elevated deformation temperatures (923−1223 K) and the high strain rates ($0.05-1.0\,s^{-1}$) on a computer controlled servo-hydraulic testing-machine, as shown in Figure 1a, which have a maximal limit to heat the specimen till 1223 K. In Figure 1a, the clamped tensile specimen is covered with the isolation part to achieve the isothermal condition and in addition, the prepared tensile specimen, which is inside the testing machine, is shown in Figure 1b for the detailed view. Before conducting the tests, as displayed in Figure 1b, the calibrations are done using the thermocouples in order to determine the heating time to obtain the uniform temperature distribution approximately for the specific temperature value and then the noted details are utilized to conduct the experiments lately. The experiments are conducted sequentially at the interval of 373 K deformation temperatures considering the four constant strain rates ranging from 0.05 to $1.0\,s^{-1}$.

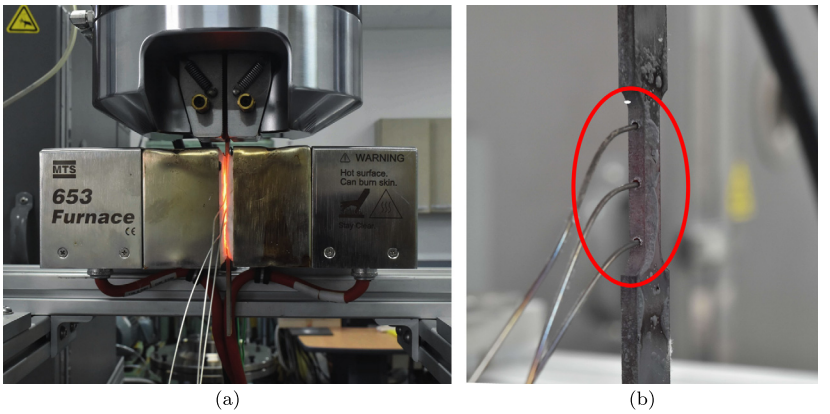

(a) (b)

Figure 1. Experimental set-up. (a) Test machine; (b) Specimen with thermocouples.

During experiment, two specimens are tested for the each case and the averaged load-stroke data are transformed into the true stress-strain data using the standard equations of the simple tensile tests.

The engineering measures of stress and strain, denoted in these articles as σ_e and ε_e, respectively, are determined from the load and displacement measured during the tensile test as follows:

$$\sigma_e = \frac{P}{A_0} \quad \text{and} \quad \varepsilon_e = \frac{\delta}{L_0} \tag{1}$$

whereas, in Eq. (1), P, A_0, δ, L_0 are the load, the original cross-section area, the displacement and the original length, respectively. Using the following Eq. (2), the true stress, σ_t, and true strain, ε_t, values can be estimated in order to include the cross-sectional area changes during the deformation:

$$\sigma_t = \sigma_e(1 + \varepsilon_e) \quad \text{and} \quad \varepsilon_t = \ln(1 + \varepsilon_e). \tag{2}$$

The fractured specimens and the obtained flow stress-strain data are displayed in Figure 2. Subsequently, the elastic region is removed from the flow curves in order to obtain the true plastic flow curves for the purpose of constitutive model parameters estimation. The highest stress values are measured at deformation temperature, 923 K, and strain rate, $1.0\,s^{-1}$, and it is because the flow stress increases as the strain rate increases and the deformation temperature decreases, and vice-versa. In detail, in high strain rate and low deformation temperature, there is no enough time to completely recrystallize during the deformation, and in other words, it can be explained as strain hardening or work hardening, which happens due to an interaction between dislocations and particles. In other hand, the stress decreases with deformation temperature due to the dynamic re-crystallization or dynamic recovery. With further decrease in strain rate and increase in temperature, the flow stress tends to decrease steadily during the deformation process and it is due to the balance between the work-hardening and thermal softening from dynamic recovery

https://doi.org/10.1016/j.heliyon.2019.e01347

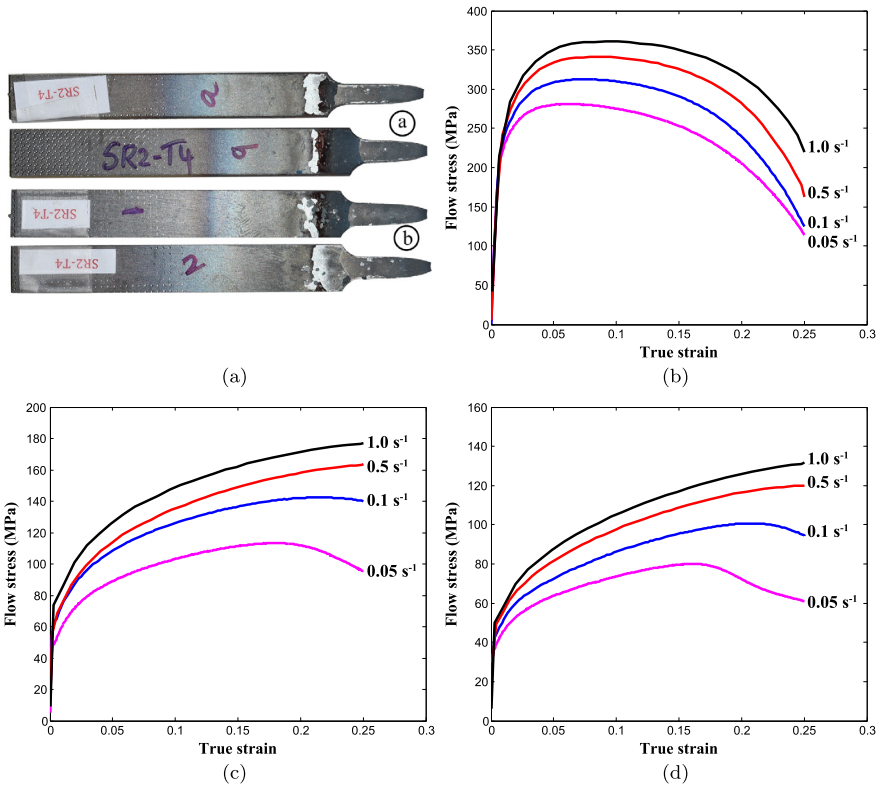

Figure 2. True strain-true stress data obtained from hot tensile tests at various temperatures under different strain rates. (a) Fractured specimens at 1223 K and 0.1 s^{-1}; (b) $T = 923$ K; (c) $T = 1123$ K; (d) $T = 1223$ K.

or recrystallization. However, Figure 2b is most evident that the plastic instability, sometimes called unstable deformation, occurred as the supportable load (in terms of stress) started to decrease after the necking initiation. It happens due to the loss of balance between increase in strength due to hardening and increase in stress due to thinning. Here it is important to note down that this behavior found to happen at low deformation temperature for an entire strain rates, Figure 2b, and low strain rates for a high deformation temperature, Figures 2c and 2d. Therefore, selecting the flow curves for the model prediction is crucial, and need more attention by considering these issues into account.

3. Results and discussion

3.1. Modified Johnson-Cook model

The flow stress-strain data from uniaxial tensile tests can be used to develop the constitutive relations and material model parameters. Among the existing empirical phenomenological models, the modified JC model is employed to characterize

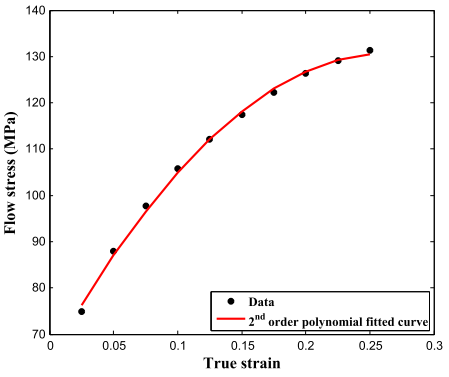

Figure 3. Relationship between σ and ε at reference conditions.

the plastic deformation behavior of AISI-1045 material under the deformation temperatures of (923−1223 K) and the strain rates of (0.05−1.0 s^{-1}). The modified JC model can be represented as follows [19,20,21]:

$$\sigma = (A_1 + B_1\varepsilon + B_2\varepsilon^2)(1 + C_1 \ln\dot{\varepsilon}^*)\exp[(\lambda_1 + \lambda_2 \ln\dot{\varepsilon}^*)T^*], \quad (3)$$
$$\dot{\varepsilon}^* = \frac{\dot{\varepsilon}}{\dot{\varepsilon}_{\text{ref}}},$$
$$T^* = T - T_{\text{ref}},$$

where σ is the equivalent flow stress, ε and $\dot{\varepsilon}$ are the equivalent plastic strain and strain rate, respectively. $\dot{\varepsilon}_{\text{ref}}$ is the reference strain rate, in this present work, it is defined as 1.0 s^{-1} according to the experimental data. T and T_{ref} are the current working temperature and reference temperature, in this present study, it is taken as 1223 K, respectively. A_1, B_1, B_2, C_1, λ_1 and λ_2 are the model material constants. In the modified JC model, the coupled effects of work hardening, strain rate hardening and thermal softening are considered. This flow stress model is elected over the original JC model based on the published information. The detailed procedures to determine the constitutive model parameters are explained below.

3.1.1. Determination of constants A_1, B_1, B_2

The model constants such as A_1, B_1 and B_2 are fitted by the flow stress data at the reference temperature, 1223 K, and the reference strain rate condition, 1.0 s^{-1}. Under reference conditions, the modified JC model, Eq. (3), can be expressed as:

$$\sigma = (A_1 + B_1\varepsilon + B_2\varepsilon^2). \quad (4)$$

As displayed in Figure 3, the strain hardening exhibits nonlinear relationship with increasing strain values. By substituting the corresponding flow stress data into Eq. (4), the material parameters such as A_1, B_1 and B_2, can be estimated from the second order polynomial equation coefficients considering only main effects

 https://doi.org/10.1016/j.heliyon.2019.e01347

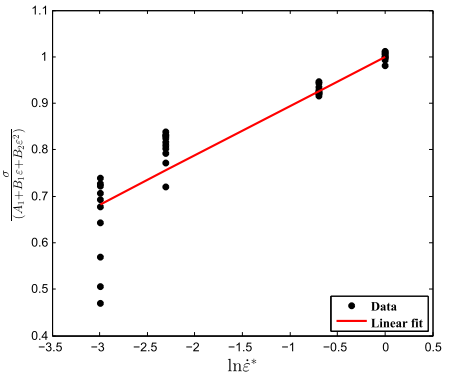

Figure 4. Relationship between $\sigma/(A_1 + B_1\varepsilon + B_2\varepsilon^2)$ and $\ln\dot{\varepsilon}^*$.

of strain. The material constants, A_1, B_1 and B_2 are determined as 64.36 MPa, 499.9 MPa and −940.3 MPa, respectively, from the coefficients of fitted polynomial equation.

3.1.2. Determination of constant C_1

Using the reference deformation temperature condition, 1223 K, and neglecting the influence of thermal softening effect, Eq. (3), can be rewritten as:

$$\sigma = (A_1 + B_1\varepsilon + B_2\varepsilon^2)(1 + C_1 \ln\dot{\varepsilon}^*)$$

$$\frac{\sigma}{(A_1 + B_1\varepsilon + B_2\varepsilon^2)} = (1 + C_1 \ln\dot{\varepsilon}^*)$$

The relationship between stress, $\frac{\sigma}{(A_1+B_1\varepsilon+B_2\varepsilon^2)}$, and the dimensionless strain rate, $\ln\dot{\varepsilon}^*$, at the reference temperature, 1223 K, can be obtained by substituting the selected experimental flow stress data at the ten discrete strain values between 0.025 and 0.25. Then the model parameter value, C_1, is determined as 0.1061 from the slope of the fitted polynomial curve as shown in Figure 4.

3.1.3. Determination of constants λ_1, λ_2

For different deformation temperatures and strain rates, Eq. (3) can be rearranged as follows:

$$\frac{\sigma}{(A_1 + B_1\varepsilon + B_2\varepsilon^2)(1 + C_1 \ln\dot{\varepsilon}^*)} = \exp[(\lambda_1 + \lambda_2 \ln\dot{\varepsilon}^*)T^*] \tag{5}$$

Taking natural logarithm of Eq. (5), we can obtain the following equation:

$$\ln\left\{\frac{\sigma}{(A_1 + B_1\varepsilon + B_2\varepsilon^2)(1 + C_1 \ln\dot{\varepsilon}^*)}\right\} = (\lambda_1 + \lambda_2 \ln\dot{\varepsilon}^*)T^* \tag{6}$$

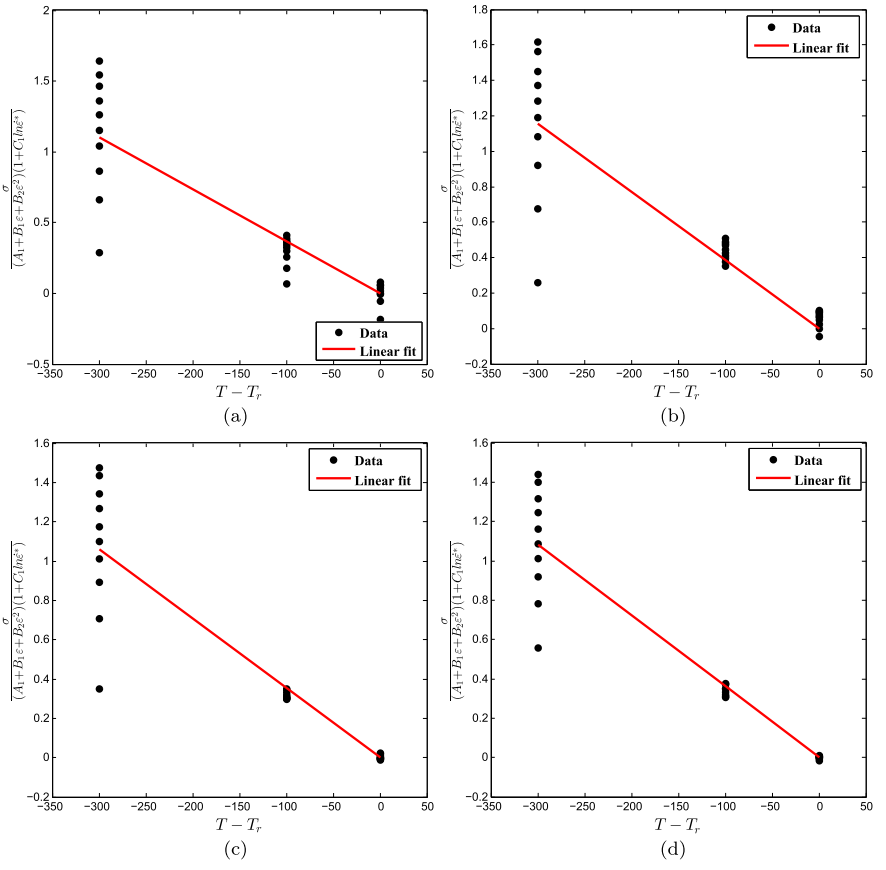

Figure 5. Relationship between $\ln\left\{\sigma/(A_1 + B_1\varepsilon + B_2\varepsilon^2)(1 + C_1 \ln\dot{\varepsilon}^*)\right\}$ and T^*. (a) $\dot{\varepsilon} = 0.05\,\mathrm{s}^{-1}$; (b) $\dot{\varepsilon} = 0.1\,\mathrm{s}^{-1}$; (c) $\dot{\varepsilon} = 0.5\,\mathrm{s}^{-1}$; (d) $\dot{\varepsilon} = 1.0\,\mathrm{s}^{-1}$.

In order to simplify Eq. (6), we are introducing the parameter, λ, is equal to $(\lambda_1 + \lambda_2 \ln\dot{\varepsilon})$, and the new parameter can be gained from the relationship between $\ln\left\{\frac{\sigma}{(A_1+B_1\varepsilon+B_2\varepsilon^2)(1+C_1 \ln\dot{\varepsilon}^*)}\right\}$ and T^*. In this present derivation, we have four different strain rates, so the four different values of λ can be achieved from the slope of the linear fitting curves as displayed in Figure 5.

$$\lambda = \lambda_1 + \lambda_2 \ln\dot{\varepsilon}$$

Subsequently, the material model parameters, λ_1 and λ_2 can be achieved from the intercept and the slope of the linear relationship between the new parameter, λ, and the dimensionless strain rate, $\ln\dot{\varepsilon}$, as shown in Figure 6. From the fitted curve, the material constants, λ_1 and λ_2 are determined as -0.00359, 8.73×10^{-5}, respectively.

Thus, the predicted constitutive equation of the modified JC model is established according to the estimated material constants as follows:

$$\hat{\sigma}_{\mathrm{pred}} = (64.36 + 499.9\varepsilon - 940.3\varepsilon^2)\left(1 + 0.1061 \ln\left(\frac{\dot{\varepsilon}}{1.0}\right)\right) \exp\left[\left(-0.00359 + 8.73\times10^{-5} \ln\left(\frac{\dot{\varepsilon}}{1.0}\right)\right)(T - 1223)\right].$$

https://doi.org/10.1016/j.heliyon.2019.e01347

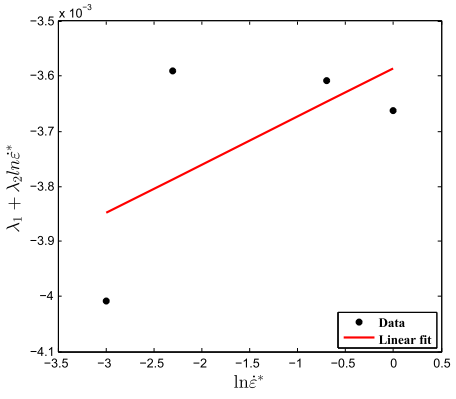

Figure 6. Relationship between λ and $\ln\dot{\varepsilon}$.

3.2. Modified Zerilli-Armstrong model

The modified ZA model for predicting the material flow behavior can be expressed as [12,22,26,28]:

$$\sigma = (C_1 + C_2\varepsilon^n)\exp[-(C_3 + C_4\varepsilon)T^* + (C_5 + C_6T^*)\ln\dot{\varepsilon}^*], \tag{7}$$

$$\dot{\varepsilon}^* = \frac{\dot{\varepsilon}}{\dot{\varepsilon}_{\text{ref}}}$$

$$T^* = T - T_{\text{ref}}$$

where σ is the equivalent flow stress, ε, $\dot{\varepsilon}$ and $\dot{\varepsilon}_{\text{ref}}$ are the equivalent plastic strain, the strain rate and the reference strain rate, respectively. T and T_{ref} are, respectively, the current working temperature and reference temperature. In Eq. (7), C_1, C_2, n, C_3, C_4, C_5 and C_6 are the material parameters. The step by step procedures to estimate the material model parameters are illustrated and explained below. Here, the material constant, C_1, is determined as 74.843 MPa from the yield stress of stress-strain data at the reference deformation temperature and strain rate conditions.

3.2.1. Determination of constants C_2 and n

At the reference strain rate, $1.0\,\text{s}^{-1}$, Eq. (7) can be rearranged into Eq. (8) as follows:

$$\sigma = (C_1 + C_2\varepsilon^n)\exp[-(C_3 + C_4\varepsilon)T^*]. \tag{8}$$

Then taking the natural logarithm of Eq. (8), we can obtain the following equation:

$$\ln\sigma = \ln(C_1 + C_2\varepsilon^n) - (C_3 + C_4\varepsilon)T^*,$$

$$I_1 = \ln(C_1 + C_2\varepsilon^n), \tag{9}$$

$$s_1 = -C_3 + C_4\varepsilon. \tag{10}$$

By substituting the associated flow stress-strain data from the experiment at the reference strain rate, $1.0\,\text{s}^{-1}$, the values of S_1 and I_1 can be determined from the slope

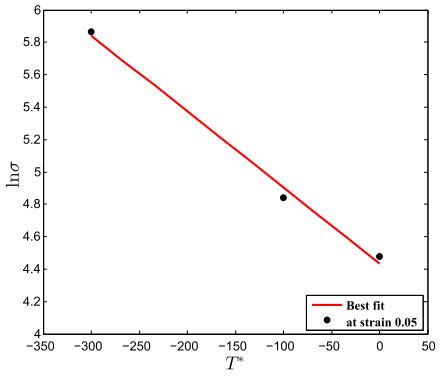

Figure 7. Relationship between $\ln\sigma$ and T^*.

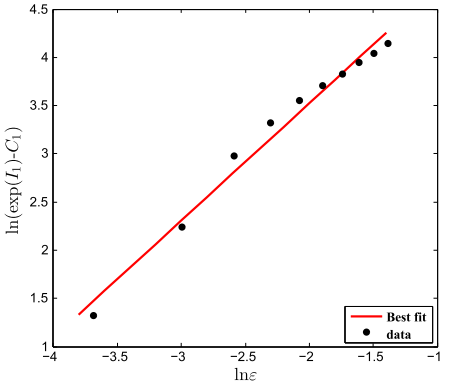

Figure 8. Relationship between $\ln(\exp(I_1) - C_1)$ and $\ln\varepsilon$.

and the intercept of the linear fitted curve between $\ln\sigma$ and T^* as shown in Figure 7. The calculation procedure for determining the values of S_1 and I_1 is repeated for the strain values between 0.05 and 0.25 at the interval of 0.025 and eventually, the ten sets of S_1 and I_1 are determined from the linear curve fitting. Further, Eq. (11) is gained by taking the natural logarithm of Eq. (9) as follows:

$$\ln(\exp(I_1) - C_1) = \ln C_2 + n\ln\varepsilon \tag{11}$$

At reference strain rate, $1.0\,s^{-1}$, considering entire deformation temperatures, substituting the values of C_1 and I_1, the linear relationship between $\ln(\exp(I_1) - C_1)$ and $\ln\varepsilon$ can be gained as illustrated in Figure 8. Thus, the material model parameters, C_2 and n are estimated as 387.998 MPa and 1.218 from the slope and the intercept of the fitted constitutive equation.

3.2.2. Determination of constants C_3 and C_4

In a similar way as we calculated the material constants, C_2 and n, at reference strain rate, $1.0\,s^{-1}$, substituting associated S_1 values to the discrete strain values,

 https://doi.org/10.1016/j.heliyon.2019.e01347

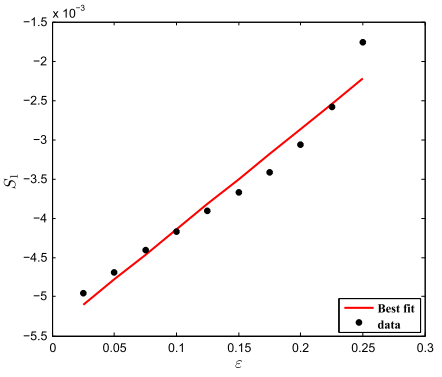

Figure 9. Relationship between S_1 and ε.

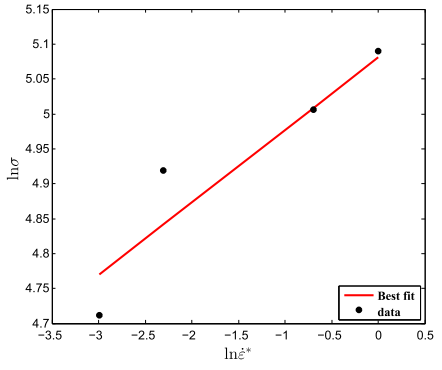

Figure 10. Relationship between $\ln\sigma$ and $\ln\dot{\varepsilon}^*$ at $\varepsilon = 0.15$ and $T = 1123$ K.

the material constants, C_3 and C_4, Eq. (10), are obtained as 0.005421 and −0.0128, respectively, from the slope and the intercept of the linear relationship between ε and S_1 as shown in Figure 9.

3.2.3. Determination of constants C_5 and C_6

Taking the natural logarithm of Eq. (7), Eq. (12) can be derived as expressed below:

$$\ln\sigma = \ln(C_1 + C_2\varepsilon^n) - (C_3 + C_4\varepsilon)T^* + (C_5 + C_6T^*)\ln\dot{\varepsilon}^*, \tag{12}$$

$$S_2 = C_5 + C_6T^* \tag{13}$$

For three deformation temperatures (923 K, 1123 K, 1223 K), the relationship between $\ln\sigma$ and $\ln\dot{\varepsilon}^*$ can be achieved as shown in Figure 10. Subsequently, the value of S_2 are obtained from the slope of the fitted curve, Figure 10, at a specific strain value. For three different temperatures, three different values of S_2 are obtained at one specified strain, for example $\varepsilon = 0.175$, and repeat the same procedure for other nine strain values. Thereafter, the material constants, C_5 and C_6, Eq. (13), can be captured from the slope and the intercept of the fitted curve between T^* and S_2 as depicted in Figure 11.

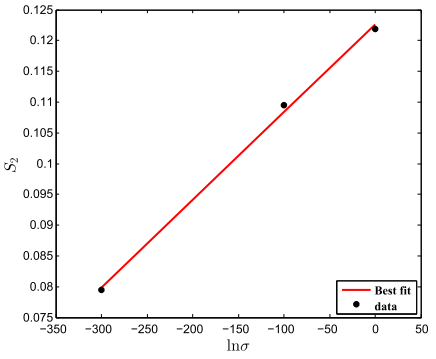

Figure 11. Relationship between S_2 and $\ln\sigma$ at $\varepsilon = 0.175$.

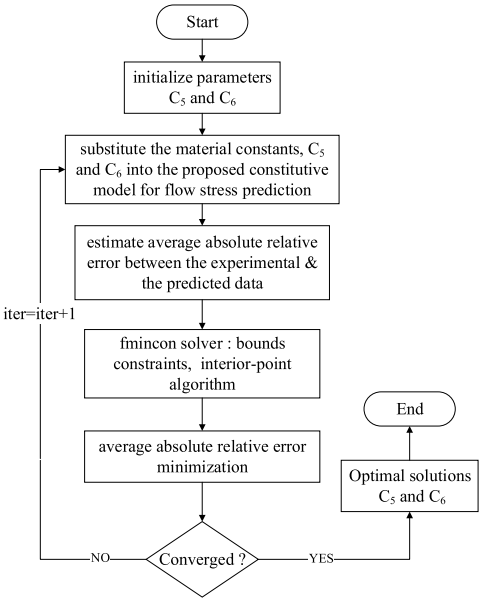

Figure 12. Flow chart of optimization procedure to find the minimum of an objective function in the presence of bound constraints.

Ten sets of material constants such as C_5 and C_6 are determined at different true strains. A bounds constrained optimization procedure (Figure 12) is employed to find the optimum solution of the material constants, C_5, C_6 and the optimization formulation employed in this present work is expressed below:

$$\begin{cases} \underset{x}{\text{Minimize:}} \\ \quad \text{AARE} = \frac{1}{n}\sum_{i=1}^{n}\left|\frac{\sigma^i_{\text{exp}} - \sigma^i_{\text{pred}}}{\sigma^i_{\text{exp}}}\right| \times 100\%, \\ \quad \text{where, } \sigma_{\text{pred}} = (C_1 + C_2\varepsilon^n)\exp[-(C_3 + C_4\varepsilon)T^* + (x(1) + x(2)T^*)\ln\dot{\varepsilon}^*] \\ \text{subjected to} \quad \begin{cases} C_{5\min} \le x(1) \le C_{5\max} \\ C_{6\min} \le x(2) \le C_{6\max} \end{cases} \end{cases}$$

Table 2. Parameters of AISI-1045 steel for the modified ZA model.

Parameter	C_1 (MPa)	C_2 (MPa)	n	C_3	C_4	C_5	C_6
Value	74.843	387.998	1.218	0.005421	-0.0128	0.1246	0.0001

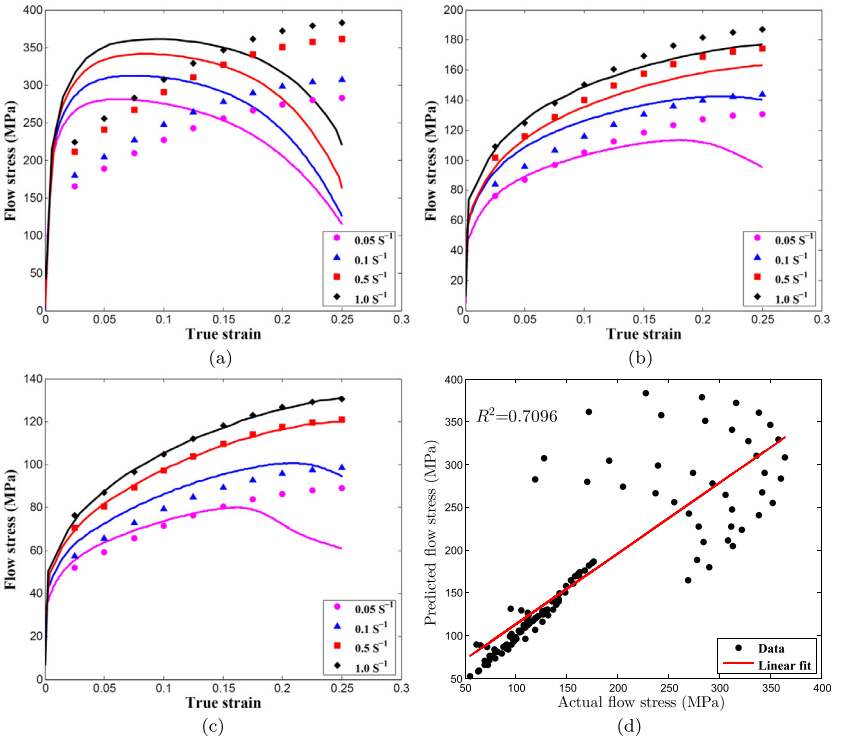

Figure 13. Comparison between experimental and predicted flow stress data using modified JC model. (a) $T = 923$ K; (b) $T = 1123$ K; (c) $T = 1223$ K; (d) Correlation plot between experimental and predicted flow stress data.

For this purpose, the nonlinear programming solver, find minimum of constrained nonlinear multivariable function (fmincon), is used with the interior-point (IP) algorithm to minimize the prediction error between measured and estimated flow stress data. For this optimization problem, the IP algorithm is used because the goal is to find the minimum of an objective function in the presence of only bounds constraints. The obtained results showed that the minimum prediction error can be achieved as 9.91%, when the material constants, C_5 and C_6, are 0.1246 and 0.0001, respectively. The estimated model constants of the modified ZA model are summarized in Table 2.

The flow stress values for the deformation temperatures, (923−1223 K), and the strain rates, (0.05−1.0 s^{-1}), are calculated with the help of computed material constants of the modified JC and the modified ZA models. Thereafter, the estimated flow stress values are compared with the measured flow stress values to check the predictability of the proposed flow stress models as displayed in Figures 13 and 14.

 https://doi.org/10.1016/j.heliyon.2019.e01347

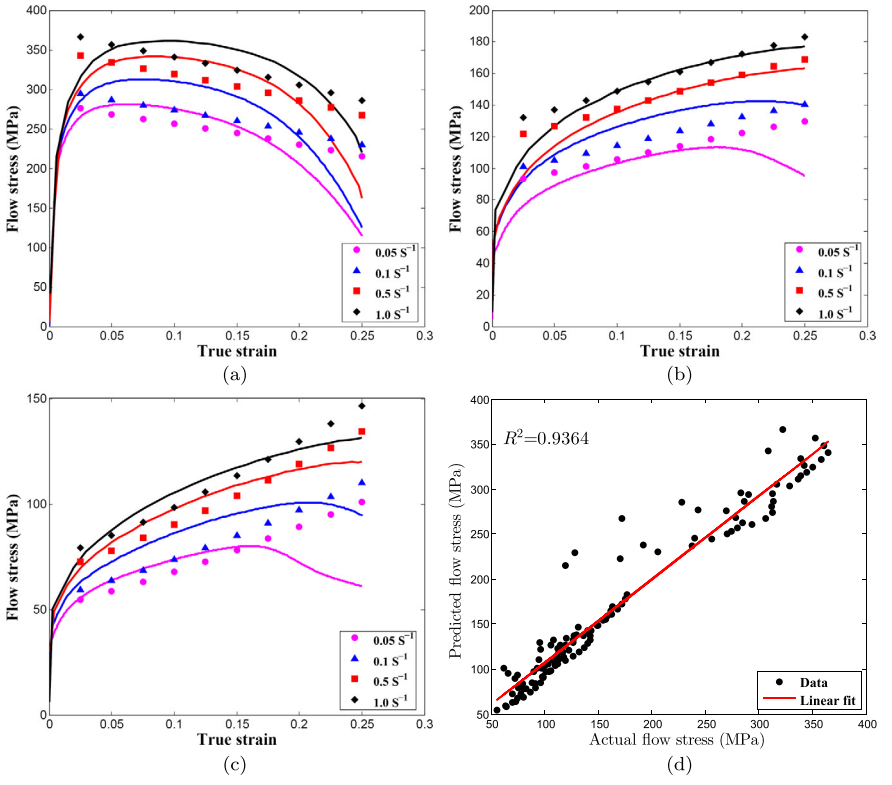

Figure 14. Comparison between experimental and predicted flow stress data using modified ZA model. (a) $T = 923$ K; (b) $T = 1123$ K; (c) $T = 1223$ K; (d) Correlation plot between experimental and predicted flow stress data.

To perform the model validation, two standard statistical measurements are used. The first metric: R^2, a statistical measure, is employed to explain the strength of linear relationship between the two variables, in this work, the two variables are the measured and the estimated observations. It is represented as a value between zero and one. If the estimated statistical measure is close to one, the model explains the better predictability between the two variables or vice versa. The model can be expressed as follows [29,30,31]:

$$R^2 = 1 - \frac{\sum_{i=1}^{n}(\sigma_{\text{exp}}^{i} - \hat{\sigma}_{\text{pred}}^{i})^2}{\sum_{i=1}^{n}(\sigma_{\text{exp}}^{i} - \bar{\sigma}_{\text{exp}})^2},$$

where σ_{exp}, σ_{pred}, $\hat{\sigma}$ and n the experimental flow stress, the predicted flow stress, the mean values of the experimental flow stress and the total number of data points, respectively. The second metric: AARE is utilized for measuring the predictability of the flow stress model through term by term comparison of the relative error [29,30,31].

 https://doi.org/10.1016/j.heliyon.2019.e01347

Table 3. Statistical measurements of modified JC model.

Conditions	R^2	Overall-R^2	AARE (%)	Overall-AARE (%)
923 K	0.0062		31.7267	
1123 K	0.9009	0.7096	6.0907	14.391
1223 K	0.8901		5.3562	

Table 4. Statistical measurements of modified ZA model.

Conditions	R^2	Overall-R^2	AARE (%)	Overall-AARE (%)
923 K	0.6804		13.0424	
1123 K	0.8454	0.9364	6.8803	9.9141
1223 K	0.7706		9.8195	

$$\mathrm{AARE} = \frac{1}{n}\sum_{i=1}^{n}\left|\frac{\sigma^{i}_{\mathrm{exp}} - \sigma^{i}_{\mathrm{pred}}}{\sigma^{i}_{\mathrm{exp}}}\right| \times 100\%,$$

where σ_{exp}, σ_{pred}, $\hat{\sigma}$ and n the experimental flow stress, the estimated flow stress, the mean value of measured data and the total number of data points, respectively. In this research, each test conditions are investigated by estimating the values of R^2 and AARE value for each case than the conventional method, in which the entire data set used to compute the statistical parameters as mentioned in Tables 3 and 4. In this way, the prediction strength of the proposed JC model can be discussed in detail. From Figures 13 and 14, overall, it is identified that the modified ZA model displayed a better relationship with the measured data in most of the test conditions than the modified JC model. This statement again proved using the numerical values which outlined in Tables 3 and 4.

In Figure 13a, the predicted flow curves and experimental flow curves show the large deviation at the deformation temperature, 923 K, for the entire set of strain rates. Using the flow stress-strain data, the relationship plot is obtained as depicted in Figure 13d. From Figure 13d, it has been noticed that the deviation of flow stress values, at the right top corner, is found to have a flower pattern behavior. This flower pattern explains that the modified JC model constants are having a negative influence on the tracking the flow behavior accurately. Furthermore, it is important to mention here that the main reason for having this prediction error owing to the plastic instability occurred during the tensile test as discussed in section 2. In addition, the same prediction error is evident from Figures 13b and 13c for the deformation temperatures, 1123 K and 1223 K, at strain rate, 0.05 s^{-1}, for the tested conditions, and this leads to the highest prediction error as listed in Table 3. However, it is evident that the modified JC model can represent the material flow behavior more accurately at the elevated temperatures (1123 K and 1223 K) and lower strain rates (0.05 s^{-1} and 0.1 s^{-1}) as shown in Figures 13b and 13c. In addition, the estimated statistical measures, AARE, and R^2, as outlined in Table 3, are utilized to demonstrate the proposed model prediction accuracy in terms of each tested conditions. As a result,

 https://doi.org/10.1016/j.heliyon.2019.e01347

Table 5. Statistical parameters estimation from random experiments at deformation temperature 1023 K.

Conditions	Models	R^2	AARE (%)
$0.05\,s^{-1}$	modified JC model	0.8681	9.61
$1.0\,s^{-1}$		0.6743	
$0.05\,s^{-1}$	modified ZA model	0.8778	4.39
$1.0\,s^{-1}$		0.7656	

the calculated values of statistical measures implies that the modified JC model is not an accurate model to perfectly describe the material flow behavior at the lower temperatures and the higher strain rates. However, the deviations are quite acceptable in the higher strain rates as it depicts the reasonable overall metrics in Table 3.

Likewise, using the modified ZA model parameters summarized in Table 2, the flow stress values are predicted for the various experimental conditions. From Figures 14b and 14c, at deformation temperatures, 1123 K and 1223 K, most of the flow stress data fall very close to the experimental data where as the considerable deviation is noticed in Figure 14a for the deformation temperature, 923 K. Consequently, the correlation plot obtained from the developed flow stress model is depicted in Figure 14d and corresponding value of the statistical parameters, R^2, and AARE are estimated as 0.9364 and 9.9141%, respectively. Figure 14d and the numerical values are evident that a good correlation between measured and estimated flow stress-strain data is obtained for an entire processing conditions. Further, the AARE of the modified ZA model, 9.9141%, is smaller than the modified JC model, 14.391%, and this shows that the modified ZA model have considerable capability to predict the flow behavior throughout the entire deformation temperature and strain rate conditions.

In addition, the random experiments are conducted at deformation temperature, 1023 K under strain rates of $0.05\,s^{-1}$ and $1.0\,s^{-1}$ to verify the proposed models adequacies. The computed model parameters of the modified JC and the modified ZA models are employed for flow stress prediction, and the obtained flow curves are depicted in Figures 15a and 15d. Comparing the estimated values with the experimental data using graphical validations, Figures 15b, 15c, 15e and 15f as well as computing the statistical parameters, Table 5, indicates that the modified ZA can predict the material behavior more accurately than modified JC model as the AARE of the modified ZA model, 4.39%, is smaller than the modified JC model, 9.61%.

$$\text{Error} = \frac{|(9.9141 - 14.391)|}{9.9141} \times 100 = 45.15\%. \tag{14}$$

Overall, it can be easily concluded, from the comparison depicted in Figures 13 and 14 and the numerical values summarized in Tables 3 and 4, that the modified ZA model is comparatively more prominent and shows better agreement between measured and estimated data than the modified JC model at the entire processing

 https://doi.org/10.1016/j.heliyon.2019.e01347

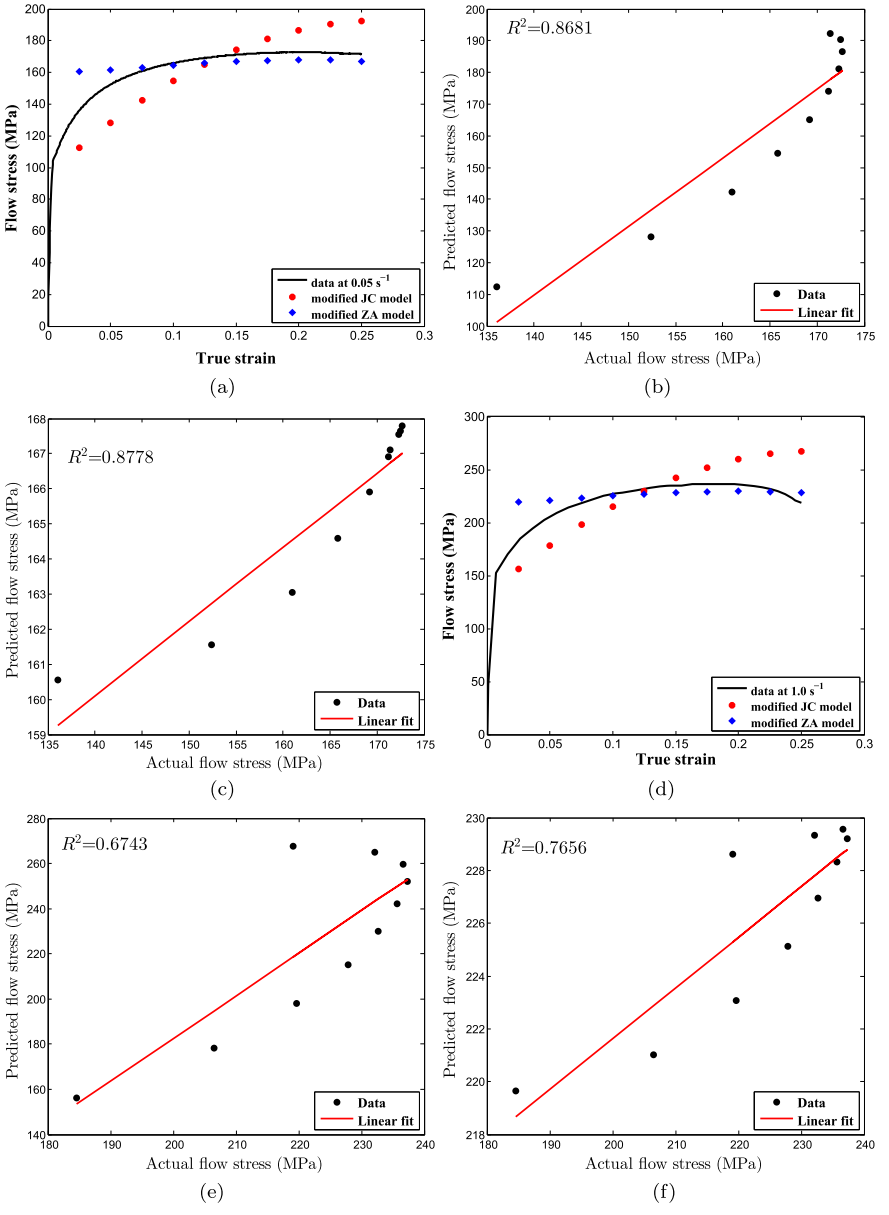

Figure 15. Random experiments to validate the proposed models. (a) $T = 1023$ K; (b) Correlation plot for modified JC model; (c) Correlation plot for modified ZA model; (d) $T = 1023$ K; (e) Correlation plot for modified JC model; (f) Correlation plot for modified ZA model.

conditions. In addition, the modified ZA model involves seven material constants, which is almost close to the number of model constants involved in the modified JC model. But, the computational time required for computing the material constants of the modified ZA model is little bit longer than the other model, because the computation of material constants, C_5 and C_6 takes a few steps of optimization procedures. Furthermore, the model prediction error percentage, Eq. (14), between the modified JC model and ZA model is determined as 45.15%. The error percentage

proves that the little longer computational time results in better outcome of flow stress prediction.

4. Conclusion

In this present work, two flow stress models have been proposed to verify the predictability of the modified JC and the modified ZA models to represent the material flow behavior of AISI-1045 steel in a wide range of deformation temperatures (923−1223 K) and strain rates (0.05−1.0 s^{-1}). From this present study, the following conclusions are made:

- The precise experiment is carried out using two different sets of specimens, and the true stress-strain data for the material model parameters estimation are computed from the averaged flow stress data.
- The modified JC model is lacking ability to provide a good tracking of material flow behavior of AISI-1045 steel at the higher strain rates and lower temperatures. The main reason of this inadequacy is due to the improper estimation of exponent term, thermal softening, in the modified JC constitutive equation.
- The modified ZA model is adequate as the predictions are well agreed with the experimental data and indicates the acceptable statistical measures, in terms of average absolute relative error and the coefficient of determination. But, this model needs more computational time to estimate the material parameters, even though the number of materials are quite same with the modified JC model. However, the modified ZA model could predict the deformation behavior much more accurately than the modified JC model.
- Random experiments are performed to verify the predictability of the proposed flow stress models, and it can be used to identify and eliminate the experimental error such as noise, change in environmental conditions and voltage fluctuations.
- The detailed step by step procedures for computing the material model parameters are presented here, and this proposed model can be utilized to develop the numerical model to replicate the real system behavior.

Declarations

Author contribution statement

Jung Dong-Won: Supervision.

 https://doi.org/10.1016/j.heliyon.2019.e01347

Mohanraj Murugesan: Conceived and designed the experiments; Performed the experiments; Analyzed and interpreted the data; Contributed reagents, materials, analysis tools or data; Wrote the paper.

Funding statement

This work was supported by the 2019 scientific promotion program funded by Jeju National University.

Competing interest statement

The authors declare no conflict of interest.

Additional information

No additional information is available for this paper.

References

[1] Z. jun Tao, X. guang Fan, H. Yang, J. Ma, H. Li, A modified Johnson-Cook model for NC warm bending of large diameter thin-walled Ti-6Al-4V tube in wide ranges of strain rates and temperatures, Trans. Nonferr. Met. Soc. China 28 (2018) 298–308.

[2] J.E. Plumeria, L. Madej, W.Z. Misiolek, Constitutive modeling and inverse analysis of the flow stress evolution during high temperature compression of a new ZE20 magnesium alloy for extrusion applications, Mater. Sci. Eng. A 740–741 (2019) 174–181.

[3] J. Guo, M. Zhan, M.W. Fub, P.F. Gao, F. Ma, Extrapolation based constitutive modeling of flow stress of titanium alloy sheet under hot-working condition, Mater. Des. 154 (2018) 96–107.

[4] J. He, F. Chen, B. Wang, L.B. Zhu, A modified Johnson-Cook model for 10% Cr steel at elevated temperatures and a wide range of strain rates, Mater. Sci. Eng. A 715 (2018) 1–9.

[5] Y.C. Lin, X.M. Chen, A critical review of experimental results and constitutive descriptions for metals and alloys in hot working, Mater. Des. 32 (2011) 1733–1759.

[6] D.G. He, Y.C. Lin, J. Chen, D.D. Chen, J. Huang, Y. Tang, M.S. Chen, Microstructural evolution and support vector regression model for an aged Ni-

based superalloy during two-stage hot forming with stepped strain rates, Mater. Des. 154 (2018) 51–62.

[7] Y.C. Lin, J. Huang, H.B. Li, D.D. Chen, Phase transformation and constitutive models of a hot compressed TC18 titanium alloy in the $\alpha + \beta$ regime, Vacuum 157 (2018) 83–91.

[8] D.-D. Chen, Y.C. Lin, Y. Zhoua, M.S. Chen, D.X. Wen, Dislocation substructures evolution and an adaptive-network-based fuzzy inference system model for constitutive behavior of a Ni-based superalloy during hot deformation, J. Alloys Compd. 708 (2017) 938–946.

[9] Y.Q. Jiang, Y.C. Lin, X.Y. Zhang, C. Chen, Q.W. Wang, G.D. Pang, Isothermal tensile deformation behaviors and fracture mechanism of Ti-5Al-5Mo-5V-1Cr-1Fe alloy in β phase field, Vacuum 156 (2018) 187–197.

[10] S. Siamak, Prediction of temperature distribution and required energy in hot forging process by coupling neural networks and finite element analysis, Mater. Lett. 61 (2007) 3296–3300.

[11] H.Y. Li, Y.H. Li, X.F. Wang, J.J. Liu, Y. Wu, A comparative study on modified Johnson Cook, modified Zerilli-Armstrong and Arrhenius-type constitutive models to predict the hot deformation behavior in 28CrMnMoV steel, Mater. Des. 49 (2013) 493–501.

[12] H. Zhang, W. Wen, H. Cui, Y. Xu, A modified Zerilli-Armstrong model for alloy IC10 over a wide range of temperatures and strain rates, Mater. Sci. Eng. A 527 (2009) 328–333.

[13] J. Cai, K. Wang, P. Zhai, F. Li, J. Yang, A modified Johnson-Cook constitutive equation to predict hot deformation behavior of Ti-6Al-4V alloy, J. Mater. Eng. Perform. 24 (2015) 32–44.

[14] A.K. Maheshwari, Prediction of flow stress for hot deformation processing, Comput. Mater. Sci. 69 (2013) 350–358.

[15] Z. Akbari, H. Mirzadeh, J.M. Cabrera, A simple constitutive model for predicting flow stress of medium carbon microalloyed steel during hot deformation, Mater. Des. 77 (2015) 126–131.

[16] Y.C. Lin, X.M. Chen, G. Liu, A modified Johnson–Cook model for tensile behaviors of typical high-strength alloy steel, Mater. Sci. Eng. A 527 (2010) 6980–6986.

[17] W. Song, J. Ning, X. Mao, H. Tang, A modified Johnson-Cook model for titanium matrix composites reinforced with titanium carbide particles at elevated temperatures, Mater. Sci. Eng. 576 (2013) 280–289.

 https://doi.org/10.1016/j.heliyon.2019.e01347

[18] H.Y. Li, X.F. Wang, J.Y. Duan, J.J. Liu, A modified Johnson Cook model for elevated temperature flow behavior of T24 steel, Mater. Sci. Eng. 577 (2013) 138–146.

[19] X. Wang, C. Huang, B. Zou, H. Liu, H. Zhu, J. Wang, Dynamic behavior and a modified Johnson–Cook constitutive model of Inconel 718 at high strain rate and elevated temperature, Mater. Sci. Eng. 580 (2013) 385–390.

[20] J.Q. Tan, M. Zhan, S. Liu, T. Huang, J. Guo, H. Yang, A modified Johnson–Cook model for tensile flow behaviors of 7050-T7451 aluminum alloy at high strain rates, Mater. Sci. Eng. 631 (2015) 214–219.

[21] Q.Y. Hou, J.T. Wang, A modified Johnson-Cook constitutive model for Mg–Gd–Y alloy extended to a wide range of temperatures, Comput. Mater. Sci. 50 (2010) 147–152.

[22] T. Mirzaie, H. Mirzadeha, J.M. Cabrerab, A simple Zerilli–Armstrong constitutive equation for modeling and prediction of hot deformation flow stress of steels, Mech. Mater. 94 (2016) 38–45.

[23] A. He, G. Xie, H. Zhang, X. Wang, A comparative study on Johnson–Cook, modified Johnson-Cook and Arrhenius-type constitutive models to predict the high temperature flow stress in 20CrMo alloy steel, Mater. Des. 52 (2013) 677–685.

[24] H. Li, L. He, G. Zhao, L. Zhang, Constitutive relationships of hot stamping boron steel B1500HS based on the modified Arrhenius and Johnson-Cook model, Mater. Sci. Eng. A 580 (2013) 330–348.

[25] G. Chen, C. Ren, Z. Ke, J. Li, X. Yang, Modeling of flow behavior for 7050-T7451 aluminum alloy considering microstructural evolution over a wide range of strain rates, Mech. Mater. 95 (2016) 146–157.

[26] H. Zhan, G. Wang, D. Kent, M. Dargusch, Constitutive modelling of the flow behaviour of a β titanium alloy at high strain rates and elevated temperatures using the Johnson–Cook and modified Zerilli–Armstrong models, Mater. Sci. Eng. 612 (2014) 71–79.

[27] U.M.R. Paturi, S.K.R. Narala, R.S. Pundir, Constitutive flow stress formulation, model validation and FE cutting simulation for AA7075-T6 aluminum alloy, Mater. Sci. Eng. 605 (2014) 176–185.

[28] D. Samantaray, S. Mandal, A.K. Bhaduri, A comparative study on Johnson-Cook, modified Zerilli-Armstrong and Arrhenius-type constitutive models to predict elevated temperature flow behaviour in modified 9Cr–1Mo steel, Comput. Mater. Sci. 47 (2009) 568–576.

[29] K. Lee, M. Murugesan, S.-M. Lee, B.-S. Kang, A comparative study on Arrhenius-type constitutive models with regression methods, Trans. Mater. Proc. 26 (2017) 18–27.

[30] M. Murugesan, B.-S. Kang, K. Lee, Multi-objective design optimization of composite stiffened panel using response surface methodology, J. Compos. Res. 28 (2015) 297–310.

[31] M. Murugesan, D.W. Jung, Johnson Cook material and failure model parameters estimation of AISI-1045 medium carbon steel for metal forming applications, Materials 12 (2019) 609–627.